# Reversible State Transition in Nanoconfined Aqueous Solutions

Liang Zhao,[1,2] Chunlei Wang,[1,*] Jian Liu,[1,2] Binghai Wen,[1,2] Yusong Tu,[3] Zuowei Wang,[4] and Haiping Fang[1,†]
[1]Laboratory of Physical Biology and Division of Interfacial Water, Shanghai Institute of Applied Physics, Chinese Academy of Sciences, Post Office Box 800-204, Shanghai 201800, China
[2]University of Chinese Academy of Sciences, Beijing 100049, China
[3]Institute of Systems Biology, Shanghai University, Shanghai 200444, China
[4]School of Mathematical and Physical Sciences, University of Reading, Whiteknights, Reading RG6 6AX, United Kingdom
(Received 22 May 2013; revised manuscript received 19 October 2013; published 20 February 2014)

Using molecular dynamics simulations, we find a reversible transition between the dispersion and aggregation states of solute molecules in aqueous solutions confined in nanoscale geometry, which is not observed in macroscopic systems. The nanoscale confinement also leads to a significant increase of the critical aggregation concentration (CAC). A theoretical model based on Gibbs free energy calculation is developed to describe the simulation results. It indicates that the reversible state transition is attributed to the low free energy barrier (of order $k_BT$) in between two energy minima corresponding to the dispersion and aggregation states, and the enhancement of the CAC results from the fact that at lower concentrations the number of solute molecules is not large enough to allow the formation of a stable cluster in the confined systems.

DOI: 10.1103/PhysRevLett.112.078301 PACS numbers: 82.70.Uv, 64.60.Q–, 07.05.Tp

The association state of solute molecules in aqueous solutions has fundamental importance in a large variety of physical and biological processes [1–7]. For instance, whether solute molecules are in the dissolved or aggregated states can strongly affect the reaction efficiency of chemical catalysis [8–11] and the functions of proteins [12,13]. The technological importance of the solute association state has also drawn extensive attention in the study of the toxicity of nanomaterials in biological cells or tissues [14,15], the fabrication of polymer nanocomposites [16], and the synthetic controlling of oxide nanomaterials [17]. In macroscopic systems, a solute molecule stays in either a stable dispersed phase or a stable aggregated phase, with some exceptions in a critical supersaturation phase [5].

Systems at nanoscales usually demonstrate physical behavior qualitatively different from that of macroscale systems, such as the incomplete local mixing in an alcohol-water mixture [3], the extra-fast flow [18,19] or gating [20,21] through nanochannels, and the surface wetting or dewetting behavior [22–26]. Nanoscale aqueous systems widely exist in biological tissues and other natural materials as well as in modern technological applications, such as the nanoscale spaces confined in between two and more biomolecules [27] and the nanoscale channels in rock gaps [28]. However, the understanding of solute aggregation behavior at nanometer sizes is still poor, although there have been extensive theoretical [29–32] and experimental [33,34] studies of systems at micrometer scales.

In this Letter, we used molecular dynamics (MD) simulations to study the aggregation behavior of aqueous solutions confined in nanoscale geometry. These simulations revealed the existence of a reversible transition between the dispersion and aggregation states of solute molecules and an enhancement of the critical aggregation concentration (CAC) in the nanoconfined systems. A theoretical model based on Gibbs free energy calculation has been proposed to interpret these distinguishing observations.

Our simulation systems consisted of various numbers of solute molecules, including pentanols ($N = 8$, 13, 15, 17, 19, 21, 25) and hexanols ($N = 7$, 10, 13, 15, 17), which were initially solvated in a cubic box of dimensions $5.20 \times 5.20 \times 5.20$ nm$^3$ containing $N_{\text{water}} = 3101$ water molecules, as shown in Fig. 1(a). All MD simulations were performed in the canonical ($NVT$) ensemble using GROMACS 4.5.4 [35]. A constant temperature of $T = 300$ K was maintained by the $v$-rescale method with a coupling time of 0.1 ps. The average pressure in the box was ~1 atm (details see PS9 in the Supplemental Material [36]). The confinement boundaries in all six directions were constructed by water walls of about 5 Å thick in which the oxygen atoms were restrained at their lattice sites by harmonic potentials. The time step was 1.0 fs and simulation data were collected every 1 ps. The particle-mesh Ewald method with a real space cutoff of 1.2 nm was used to treat the long-range electrostatic interactions, whereas the van der Waals (vdW) interactions were truncated at a cutoff distance of 1.2 nm. The GROMOS force field [37] and extended simple point charge water model were used. We denoted the $CH_3$ or $CH_2$ groups by "C" and treated them as the same entity with the Lennard-Jones parameters $\epsilon_{CC} = 0.14$ kcal/mol and $\sigma_{CC} = 3.97$ Å. $\epsilon_{OO} = 0.17$ kcal/mol and $\sigma_{OO} = 3.12$ Å. We used Stillinger's criterion [38] to define the aggregation

 © 2014 American Physical Society

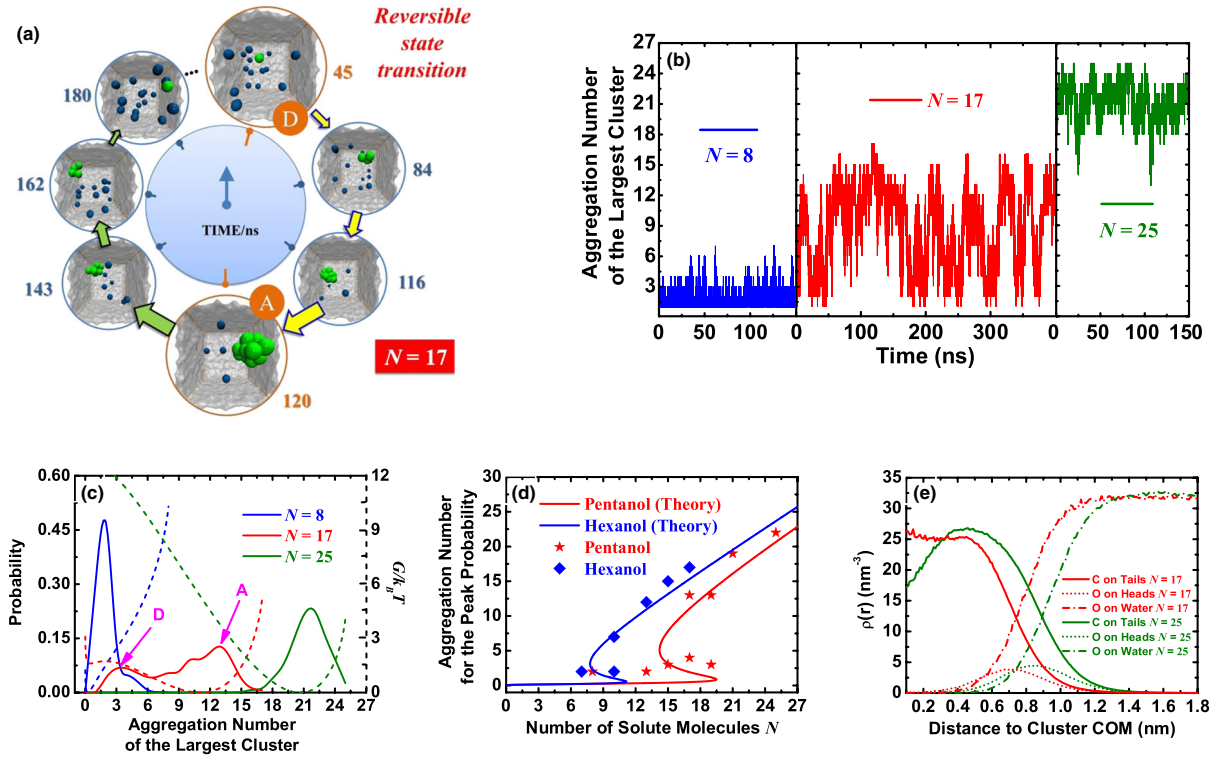


FIG. 1 (color online). States of the solute molecules. (a) Representative snapshots with the number of pentanol molecules $N = 17$. The dispersed pentanol molecules are shown in blue, and the clustered pentanol molecules are shown in green. The water walls are shown as transparent. Water molecules in the box are omitted for clarity. The typical dispersion state and aggregation state are marked by $D$ and $A$, respectively. (b) Evolution of the typical dispersion state, reversible transition between two states, and the aggregation state. (c) Probability distribution (solid lines) of the aggregation number of the largest pentanol cluster $n_{\mathrm{LC}}$ during the simulations and the theoretical results on the Gibbs free energy (dashed lines corresponding to right dashed axis) as a function of the $n_{\mathrm{LC}}$ for $N = 8$, 17, and 25. The aggregation number of the largest cluster corresponding to the peak probability is denoted by $n_{\mathrm{MPC}}$. The two probability peaks for $N = 17$ are marked by $D$ and $A$. All the minima in the energy curves are shifted to 0 for easy comparison. (d) Values of $n_{\mathrm{MPC}}$ as a function of the number of pentanol and hexanol molecules $N$. Red stars and line correspond to $n_{\mathrm{MPC}}$ and the fitting line for pentanol, and blue diamonds and line represent $n_{\mathrm{MPC}}$ and the fitting line for hexanol. (e) Density distribution functions $\rho(r)$ of all the C atoms on the tails (solid lines) and oxygen atom on the heads (dotted lines) of the pentanol molecules consisting of the largest cluster, and the oxygen atom on the water molecules (dash-dotted lines) surrounding the largest cluster.

state (for details see PS10 in the Supplemental Material [36]), in which two molecules were assumed to belong to the same cluster if any two C atoms from these molecules were at a distance less than $R_d = 1.5\sigma_{\mathrm{CC}} \approx 6$ Å [39].

Figure 1(a) presents some representative snapshots of the system with $N = 17$ at various times. Starting from a dispersion state with completely separated solute molecules at $t = 45$ ns, a cluster appears at later times, whose size increases gradually at $t = 84$ and 116 ns and finally reaches a value of 17, corresponding to a fully aggregated state. To our surprise, different from what would be expected in the macroscopic systems, as time further increases, the size of the cluster decreases at $t = 143$ and 162 ns, and goes back to the fully dispersed state again at $t = 180$ ns. This clearly indicates that in the nanoconfined system the state of the solute molecules can reversibly change in between the dispersion and aggregation states. In Fig. 1(b), we show the aggregation number of the largest cluster in the system $n_{\mathrm{LC}}$ as a function of time. It can be seen that $n_{\mathrm{LC}}$ fluctuates in between two plateau values $n_{\mathrm{LC}} = 2$ and 13 in a stepwise manner over a time period of 400 ns. For comparison, simulation results for the cases of $N = 8$ and 25 are also shown in Fig. 1(b). Over the entire period of simulation time, $n_{\mathrm{LC}}$ is about 2 for $N = 8$ and about 22 for $N = 25$, indicating that the solute molecules are either in a single dispersed state for $N = 8$ or in a single aggregated state for $N = 25$, rather than switching in between these two states. For convenience, we denote the value of $n_{\mathrm{LC}}$ at the probability peaks as $n_{\mathrm{MPC}}$. As shown in Fig. 1(c), when $N$ is relatively small or large enough, there is only one peak in the probability distribution curve as $n_{\mathrm{MPC}} = 2$ for $N = 8$ and $n_{\mathrm{MPC}} = 22$ for $N = 25$, corresponding to the single stable dispersion or aggregation state, respectively. For $N = 17$, there is a valley with a minimum at $n_{\mathrm{LC}} = 6$ between the peaks at $n_{\mathrm{MPC}} = 4$ and 13. We thus consider the system in a

dispersion state when $n_{LC} \leq 6$ and in an aggregation state if $n_{LC} > 6$. We note that the probability magnitude between these two peaks is still considerably large, reflecting that the switch between the dispersion and aggregation states does not occur abruptly, as can be seen in Fig. 1(b). The wide probability distribution of $n_{LC}$ values marks the variation of the cluster size during the transition process. We have analyzed the density distribution functions $\rho(r)$ of various atoms in the typical stable aggregation state for $N = 25$ and the metastable aggregation state for $N = 17$. As shown in Fig. 1(e), the C atoms on the hydrophobic tails of the pentanol molecules prefer to stay in the internal region of the clusters and the oxygen atoms on the hydrophilic heads like to stay in the external region of the clusters. The considerably wide intervals between the density distribution function peaks of the C atoms and the oxygen atoms on hydrophilic heads, 0.45 to 0.85 nm for $N = 25$, and 0.45 to 0.7 nm for $N = 17$, indicate the roughness of the interfacial regions between the tails and heads owing to thermal fluctuations.

The simulation results in Figs. 1(b) and 1(c) show a strong dependence on the total number, or, equivalently, the concentration, of solute molecules in the confined solutions. Figure 1(d) presents the simulation data on $n_{MPC}$ as a function of $N$. We can see that $n_{MPC} \leq 3$ for $N \leq 15$, $n_{MPC} \approx N$ for $N \geq 21$ and $n_{MPC}$ has two values in the interval of $17 \leq N \leq 19$. Therefore three solute association regimes can be clearly distinguished: a dilute regime where all solute molecules are in dispersed state, an intermediate regime with a signature of reversible dispersion-aggregation state transition, and an aggregation regime with large cluster formation. The last regime corresponds to the saturated solutions in macroscopic systems where above CAC the extra solute molecules precipitate from the solution, leading to a coexistence of the dispersed and condensed phases. We note that the CAC of pentanol is 0.25 mol/l at the macroscopic scale. But in the confined geometry, the CAC value, which is defined as the concentration at the crossover point of $N = 21$ between the second and third regimes in Fig. 1(d), is much larger, given to be 0.47 mol/l as computed from $N = 21$ and $N_{water} = 3101$.

To further explore the system size effect on the aggregation behavior, we performed additional simulations for enlarged systems, using the number of water molecules $N_{water} = 6202$ and $N_{water} = 9303$, respectively (see details in PS3 in the Supplemental Material [36]). Again we found the reversible state transition for the systems with $N = 24$ in $N_{water} = 6202$ and $N = 37$ in $N_{water} = 9303$, while at higher solute concentrations most of the molecules form a single cluster, e.g., in the cases of $N = 26$ in $N_{water} = 6202$ and $N = 40$ in $N_{water} = 9303$, respectively. The corresponding CAC values are found to be 0.277 and 0.283 mol/l. Those values together with the CAC of 0.47 mol/l for the system with $N_{water} = 3101$ show that the CAC decreases as the size of the system increases.

The existence of the reversible state transition might be universal. We have studied another solute molecule, hexanol, and performed MD simulations in which all the other settings were unchanged from that used in Figs. 1(a)–1(c). As shown in Fig. 1(d) the reversible state transition in such systems happened for $N = 10$.

Now we construct a theoretical model to describe the state transition behavior of an aqueous solution confined at nanoscale. We assume that the solute molecules can be classified into two groups: one group consisting of $n$ molecules that aggregate into a single cluster, and the other group consisting of $n_f$ dispersed molecules, under the restriction of $n + n_f = N$. According to the chemical equilibrium condition that rules the balance between these two groups of molecules, the functional relation between $n$ and $N$, namely, $n(N)$, can be written as follows (detailed derivations can be found in PS5 in the Supplemental Material [36]):

$$\begin{aligned}&\left\{\frac{8\pi}{3k_BT}\left(\frac{3v_m}{4\pi}\right)^{2/3} n^{-1/3}\gamma_{hw\infty}\left[1-\delta_{hw}\left(\frac{3v_m}{4\pi}n\right)^{-1/3}\right]\right.\\&\quad+\frac{\gamma_{w\infty}}{k_BT}a^2\left[1-\frac{4}{3}\delta_w\left(\frac{3v_m}{4\pi}n\right)^{-1/3}\right]\\&\quad\left.-\frac{\gamma_{hw\infty}}{k_BT}a^2\left[1-\frac{4}{3}\delta_{hw}\left(\frac{3v_m}{4\pi}n\right)^{-1/3}\right]\right\}\\&\quad+b\times\frac{5}{3}\left(\frac{a}{l}\right)^{4/3}n^{2/3}+\left(\frac{-\Delta\mu_{\text{transfer}}-B}{k_BT}\right)\\&=\ln\left(\frac{N-n}{V}\right).\end{aligned}\tag{1}$$

The Gibbs free energy $G$ of the joint system is

$$\begin{aligned}G=&\left\{4\pi\left(\frac{3v_m}{4\pi}\right)^{2/3}n^{2/3}\gamma_{hw\infty}\left[1-2\delta_{hw}\left(\frac{3v_m}{4\pi}n\right)^{-1/3}\right]\right.\\&+na^2\gamma_{w\infty}\left[1-2\delta_w\left(\frac{3v_m}{4\pi}n\right)^{-1/3}\right]\\&\left.-na^2\gamma_{hw\infty}\left[1-2\delta_{hw}\left(\frac{3v_m}{4\pi}n\right)^{-1/3}\right]\right\}\\&+n(-\Delta\mu_{\text{transfer}})+b\left(\frac{a}{l}\right)^{4/3}k_BTn^{5/3}\\&+\left[k_BT(N-n)\ln\left(\frac{N-n}{V}\right)-k_BT(N-n)+B(N-n)\right],\end{aligned}\tag{2}$$

where the terms inside the curly brackets are the surface energy contributions from the hydrophobic tails ($-C_4H_9$ for pentanol or $-C_5H_{11}$ for hexanol) on the surface of the cluster. The second term corresponds to the transferring energy of the hydrophobic tails from the water environment into the cluster interior [40], the third term is the free energy cost for attaching the hydrophilic heads ($-CH_2OH$) of the

pentanol or hexanol molecules to the hydrophobic tails, and the fourth term is the free energy of the dispersed molecules [29]. $\gamma_{w\infty}$ and $\gamma_{hw\infty}$ are the macroscopic interfacial tension coefficients for the water-vapor and hydrophobic-tail–water [40]; $\delta_{hw}$ and $\delta_w$ are Tolman lengths [41,42] characterizing the deviations of interfacial tensions from the corresponding macroscopic values; $v_m$ is the single molecule volume with the width and length of the hydrophobic tail denoted by $a$ and $l$; $-\Delta\mu_{\text{transfer}}$ is the transferring energy of a single hydrophobic tail from the water into the hydrophobic parts of the cluster [40]; $V$ is the volume of the system excluding the walls; and $B$ is a free constant from the chemical potential of the dispersed molecules. Here, the confinement effect mainly comes from the limited number of solute and the limited volume (for details see PS12 in the Supplemental Material [36]). It should also be noted that, different from the theories for surfactant micelles [e. g., Ref. [40] ], for the cluster studied here, the area of the hydrophilic heads on the cluster surface has been excluded from the hydrophobic-tail–water interface, and the Tolman length has been introduced to characterize the microscopic interfacial tension.

For the aqueous solutions of pentanol we solve Eq. (1) using the parameter $\gamma_{hw\infty} = 49.53$ mN/m (for details see PS4 in the Supplemental Material [36]). The dimensions of the hydrophobic tail are taken to be $a = 2.60$ Å and $l = 5.97$ Å, respectively. Furthermore, $\gamma_{w\infty} = 72$ mN/m, $\delta_w = 0.25$ Å [4]; and the parameters $\delta_{hw} = 1.23$ Å, $b = 0.02$, and $-\Delta\mu_{\text{transfer}} - B = -5.26k_BT$ are determined from the best fit. The theoretical predictions are consistent with the simulation data on $n_{\text{MPC}}$, as shown in Fig. 1(d) and the average value $\langle n_{\text{LC}} \rangle$. Similar results were achieved for larger systems as reported in the Supplemental Material [36]. Moreover, we have also observed the good agreement between theoretical and simulation data in the case of hexanol [see Fig. 1(d)]. There the input parameters are taken to be $\gamma_{hw\infty} = 52.93$ mN/m (see PS4 in the Supplemental Material [36]), $a = 2.60$ and $l = 7.27$ Å, and the fitted parameters are $\delta_{hw} = 0.99$ Å, $b = 0.02$, and $-\Delta\mu_{\text{transfer}} - B = -6.82k_BT$.

In Fig. 1(c), we also show the Gibbs free energy calculated from Eq. (2) for the pentanol system as a function of $n_{\text{LC}}$. For $N = 17$, there are two local minimum values and one maximum value. The two minima correspond to the two states of $n \approx 1$ and $n \approx 11$, respectively. Those values are very close to the values of $n_{\text{MPC}} = 4$ and 13 obtained from MD simulations. Interestingly, the energy barrier between those two minima is only $1.73k_BT$, which allows the transition between the two states to occur under thermal fluctuations and is therefore the physical origin of the simulation observations. In contrast, for $N = 8$ and 25 there is only one minimum in each free energy curve, consistent with the single state of dispersion ($N = 8$) or aggregation ($N = 25$) observed in the MD simulations.

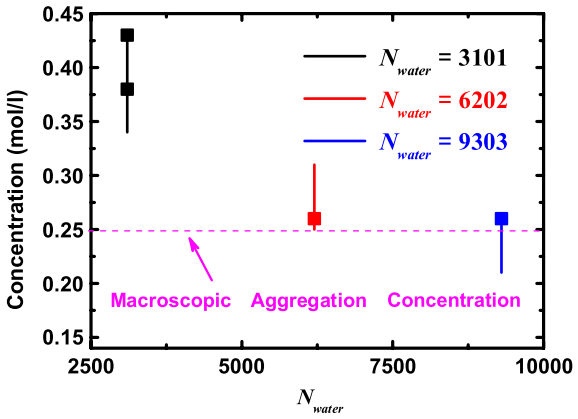


FIG. 2 (color online). Solute concentrations at which the reversible state transition occurs as a function of the number of water molecules $N_{\text{water}}$. The solid short vertical lines and the square symbols are the results from the theoretical calculations and MD simulations, respectively. The horizontal dashed line is the macroscopic critical aggregation concentration calculated from the macroscopic solubility.

Figure 2 presents the solute concentrations at which the reversible state transition occurs with respect to the number of water molecules $N_{\text{water}}$ in the system. We can see that the range of such concentrations represented by the length of the vertical lines shrinks as the size of the system increases. This implies that the reversible state transition is more difficult to be observed in larger confined systems and should vanish at macroscopic scales. When getting the results in Fig. 2 we have used an energy criterion for judging the existence of the reversible state transition, that is, the free energy barrier between the dispersion and aggregation states is less than $5k_BT$. It is noted that in our model the cluster is assumed to take a spherical shape, which limits the total number of solute molecules that can be accommodated. For pentanol this upper limit is around 55. That may lead to large error bars for the predictions made for $n_{\text{LC}}$ close to 55, and is probably the reason for the state transition concentration range predicted for $N_{\text{water}} = 9303$ being lower than the macroscopic CAC value.

In summary, we have shown a reversible dispersion-aggregation state transition and an enhancement of the critical aggregation concentration in aqueous solutions confined at nanoscale. We note that the reversible state transition has never been reported under nanoconfined geometry despite extensive theoretical, simulation, and experimental works on the association behavior of molecules and colloidal particles.

The importance of this work can be seen from the fact that the confinement of aqueous solutions at nanoscale occurs very frequently in both biological and natural environments. For example, the aggregation of ligand molecules in confined space may prevent the binding between functional hydrophobic groups and proteins. The possible toxicity of SWCNTs also depends on whether

they are dispersed or aggregated [14]. Oil usually exists in nanoscale space in the underground rock, and the aggregation property of the injected amphiphilic surfactant molecules will reduce the efficiency of oil extraction [43]. In the nanoporous media—soil, the aggregation process of minerals or nanoparticles can initiate the restoration of the carbon element and improves the activity of the soil [44].

This work was supported by NNSFC under Grants No. 10825520, No. 11204341, and No. 11105088, KIPCAS, the Shanghai Supercomputer Center of China and the Supercomputing Center of the Chinese Academy of Sciences.

*wangchunlei@sinap.ac.cn
†fanghaiping@sinap.ac.cn

[1] J. N. Israelachvili, *Intermolecular and Surface Forces: Revised Third Edition* (Academic, New York, 2011).
[2] P. Ball, Chem. Rev. **108**, 74 (2008).
[3] S. Dixit, J. Crain, W. C. Poon, J. L. Finney, and A. K. Soper, Nature (London) **416**, 829 (2002).
[4] H. S. Ashbaugh and L. R. Pratt, Rev. Mod. Phys. **78**, 159 (2006).
[5] T. M. Raschke, J. Tsai, and M. Levitt, Proc. Natl. Acad. Sci. U.S.A. **98**, 5965 (2001).
[6] A. Navrotsky, Proc. Natl. Acad. Sci. U.S.A. **101**, 12096 (2004).
[7] R. Demichelis, P. Raiteri, J. D. Gale, D. Quigley, and D. Gebauer, Nat. Commun. **2**, 590 (2011).
[8] P. Herves, M. Perez-Lorenzo, L. M. Liz-Marzan, J. Dzubiella, Y. Lu, and M. Ballauff, Chem. Soc. Rev. **41**, 5577 (2012).
[9] S. A. Bode, I. J. Minten, R. J. Nolte, and J. J. Cornelissen, Nanoscale **3**, 2376 (2011).
[10] Y. Liang, M. Ozawa, and A. Krueger, ACS Nano **3**, 2288 (2009).
[11] M. Flytzani-Stephanopoulos and B. C. Gates, Annu. Rev. Chem. Biomol. Eng. **3**, 545 (2012).
[12] P. Das, J. A. King, and R. Zhou, Proc. Natl. Acad. Sci. U.S.A. **108**, 10514 (2011).
[13] M. Ahmad, W. Gu, and V. Helms, Angew. Chem., Int. Ed. **47**, 7626 (2008).
[14] S. Liu, L. Wei, L. Hao, N. Fang, M. W. Chang, R. Xu, Y. Yang, and Y. Chen, ACS Nano **3**, 3891 (2009).
[15] S. M. Hussain, L. K. Braydich-Stolle, A. M. Schrand, R. C. Murdock, K. O. Yu, D. M. Mattie, J. J. Schlager, and M. Terrones, Adv. Mater. **21**, 1549 (2009).
[16] J. Liu, Y. Gao, D. Cao, L. Zhang, and Z. Guo, Langmuir **27**, 7926 (2011).
[17] G. R. Patzke, Y. Zhou, R. Kontic, and F. Conrad, Angew. Chem., Int. Ed. Engl. **50**, 826 (2011).
[18] K. Falk, F. Sedlmeier, L. Joly, R. R. Netz, and L. Bocquet, Langmuir **28**, 14261 (2012).
[19] W. Gu, B. Zhou, T. Geyer, M. Hutter, H. Fang, and V. Helms, Angew. Chem., Int. Ed. **50**, 768 (2011).
[20] J. Li, X. Gong, H. Lu, D. Li, H. Fang, and R. Zhou, Proc. Natl. Acad. Sci. U.S.A. **104**, 3687 (2007).
[21] Y. Tu, P. Xiu, R. Wan, J. Hu, R. Zhou, and H. Fang, Proc. Natl. Acad. Sci. U.S.A. **106**, 18120 (2009).
[22] S. Meng, L. F. Xu, E. G. Wang, and S. W. Gao, Phys. Rev. Lett. **89**, 176104 (2002).
[23] X. F. Gao, and L. Jiang, Nature (London) **432**, 36 (2004).
[24] C. Wang, H. Lu, Z. Wang, P. Xiu, B. Zhou, G. Zuo, R. Wan, J. Hu, and H. Fang, Phys. Rev. Lett. **103**, 137801 (2009).
[25] C. Wang, B. Zhou, Y. Tu, M. Duan, P. Xiu, J. Li, and H. Fang, Sci. Rep. **2**, 358 (2012).
[26] J. Trice, C. Favazza, D. Thomas, H. Garcia, R. Kalyanaraman, and R. Sureshkumar, Phys. Rev. Lett. **101**, 017802 (2008).
[27] N. Giovambattista, C. F. Lopez, P. J. Rossky, and P. G. Debenedetti, Proc. Natl. Acad. Sci. U.S.A. **105**, 2274 (2008).
[28] D. Argyris, D. R. Cole, and A. Striolo, ACS Nano **4**, 2035 (2010).
[29] J. Wedekind, D. Reguera, and R. Strey, J. Chem. Phys. **125**, 214505 (2006).
[30] T. Kaneko, T. Akimoto, K. Yasuoka, A. Mitsutake, and X. C. Zeng, J. Chem. Theory Comput. **7**, 3083 (2011).
[31] S. A. Sanders, M. Sammalkorpi, and A. Z. Panagiotopoulos, J. Phys. Chem. B **116**, 2430 (2012).
[32] N. Arai, K. Yasuoka, and X. Zeng, J. Am. Chem. Soc. **130**, 7916 (2008).
[33] D. J. Kraft, R. Ni, F. Smallenburg, M. Hermes, K. Yoon, D. A. Weitz, A. van Blaaderen, J. Groenewold, M. Dijkstra, and W. K. Kegel, Proc. Natl. Acad. Sci. U.S.A. **109**, 10787 (2012).
[34] H. Chan, A. Demortiere, L. Vukovic, P. Kral, and C. Petit, ACS Nano **6**, 4203 (2012).
[35] B. Hess, C. Kutzner, D. van der Spoel, and E. Lindahl, J. Chem. Theory Comput. **4**, 435 (2008).
[36] See Supplemental Material at http://link.aps.org/supplemental/10.1103/PhysRevLett.112.078301 for more detailed simulation data for the aqueous solutions and more discussions on the theoretical model.
[37] W. Van Gunsteren and H. Berendsen, GROMOS-87 manual. Biomos BV Nijenborgh 4, 9747 AG Groningen, Netherlands, 1987.
[38] J. F. H. Stillinger, J. Chem. Phys. **38**, 1486 (1963).
[39] J. Wedekind and D. Reguera, J. Chem. Phys. **127**, 154516 (2007).
[40] L. Maibaum, A. R. Dinner, and D. Chandler, J. Phys. Chem. B **108**, 6778 (2004).
[41] R. C. Tolman, J. Chem. Phys. **17**, 333 (1949).
[42] S. Prestipino, A. Laio, and E. Tosatti, Phys. Rev. Lett. **108**, 225701 (2012).
[43] L. L. Schramm, *Surfactants: Fundamentals and Applications in the Petroleum Industry* (Cambridge University Press, Cambridge, England, 2000).
[44] N. Perdrial, J. N. Perdrial, J. E. Delphin, F. Elsass, and N. Liewig, Eur. J. Soil Sci. **61**, 456 (2010).